ADVANCED ELECTRONIC MATERIALS Open Access
www.advelectronicmat.de

Spatially Distributed Ramp Reversal Memory in VO_2

*Sayan Basak, Yuxin Sun, Melissa Alzate Banguero, Pavel Salev, Ivan K. Schuller, Lionel Aigouy, Erica W. Carlson, and Alexandre Zimmers**

Ramp-reversal memory has recently been discovered in several insulator-to-metal transition materials where a non-volatile resistance change can be set by repeatedly driving the material partway through the transition. This study uses optical microscopy to track the location and internal structure of accumulated memory as a thin film of VO_2 is temperature cycled through multiple training subloops. These measurements reveal that the gain of insulator phase fraction between consecutive subloops occurs primarily through front propagation at the insulator-metal boundaries. By analyzing transition temperature maps, it is found, surprisingly, that the memory is also stored deep inside both insulating and metallic clusters throughout the entire sample, making the metal-insulator coexistence landscape more rugged. This non-volatile memory is reset after heating the sample to higher temperatures, as expected. Diffusion of point defects is proposed to account for the observed memory writing and subsequent erasing over the entire sample surface. By spatially mapping the location and character of non-volatile memory encoding in VO_2, this study results enable the targeting of specific local regions in the film where the full insulator-to-metal resistivity change can be harnessed in order to maximize the working range of memory elements for conventional and neuromorphic computing applications.

1. Introduction

The insulator-metal transition (IMT) in oxides is an intensely investigated phenomenon that has received considerable attention from the basic research community[1] and has the potential to revolutionize applications in electronics, smart optics, energy technologies, data storage, and neuromorphic circuits.[2] Specifically for neuromorphic applications, finding a single material that enables building both artificial synapses (plastic non-volatile memories) and neurons (nonlinear signal processing combined with volatile memory) can be highly beneficial to achieve large scale dense integration in hardware-level neural networks. Vanadium dioxide, VO_2, has emerged as a promising neuromorphic material owing to its two unique properties: (i) it undergoes a first-order thermally induced IMT at 340 K[3] (i.e., just above room temperature) in which the resistivity changes by several orders of magnitude and is accompanied by a monoclinic to tetragonal structural change; (ii) like a handful of other strongly correlated materials,[4–8] VO_2 has shown clear phase separation during its IMT,[6] that could potentially be manipulated and controlled.[9]

Recently, by patterning VO_2 and metallic leads in a particular microscale geometry, this material has been reported to show neuron characteristics such as Leaky-Integrate-and-Fire (LIF) properties[10–12] and also a ReLU activation function.[13] In contrast with these neuron-like behaviors (associated with "volatile memory"), only a few studies report the "non-volatile memory" needed to mimic synaptic behaviors in VO_2.[14–17] Recent progress was made in 2017, by applying a particular temperature sequence (the so-called "ramp

S. Basak, Y. Sun, E. W. Carlson
Department of Physics and Astronomy
Purdue University
West Lafayette, IN 47907, USA
S. Basak, Y. Sun, E. W. Carlson
Purdue Quantum Science and Engineering Institute
West Lafayette, IN 47907, USA

The ORCID identification number(s) for the author(s) of this article can be found under https://doi.org/10.1002/aelm.202300085

DOI: 10.1002/aelm.202300085

M. A. Banguero, L. Aigouy, A. Zimmers
Laboratoire de Physique et d'Étude des Matériaux
ESPCI Paris, PSL Université, CNRS
Sorbonne Université
Paris 75005, France
E-mail: azimmers@espci.fr
P. Salev
Department of Physics and Astronomy
University of Denver
Denver, Colorado 80208, USA
P. Salev, I. K. Schuller
Department of Physics and Center for Advanced Nanoscience
University of California-San Diego
La Jolla, California 92093, USA

reversal" protocol of subloops inside the main hysteresis loop), which revealed a new multi-level, *non-volatile memory* effect evidenced by a ≈20% increase in resistivity.[15] This memory effect was also found in $NdNiO_3$[15] and recently in V_2O_3.[18] A possible microscopic mechanism for this multi-level memory using "scars" at phase boundary was put forward but remains to be verified.

To clearly reveal the location of these incremental, non-volatile changes occurring in VO_2, we take advantage of the optical contrast in this material during its phase transition and report detailed optical surface maps as memory is recorded in the material. By employing high-resolution (≈400 nm) optical microscopy to image the metal/insulator phase separation state, we were able to track for the first time the creation and annihilation of metal and insulator patches while varying the temperature according to the same ramp reversal protocol as in the previously reported resistivity paper.[15] A clear buildup of mostly insulator patches was observed as multiple subloops were performed. Erasing these extra patches was achieved after ramping up the sample to high temperatures. The "scar model," previously developed to explain the change in resistivity curves during the ramp reversal protocol,[15] proposes that "scars" form at the location of the metal-insulator boundaries at each TH (high temperature turning point of the subloops). Like levees that naturally build higher riverbanks as a river's water level repeatedly rises and falls, these scars form everywhere the metallic domains change from growing to shrinking. However, we find that memory accumulates throughout the entire sample, rather than only at places where the clusters advance and then turn around, which requires some physics beyond the scar model in order to explain. Informed by these new spatially resolved experimental observations, we propose that diffusion of point defects throughout the entirety of the film can account for the ramp reversal memory effect.

Our experimental and theoretical findings light a clear path for how VO_2 can be best tailored into an artificial synapse. Previous measurements showed at most 20% ramp reversal memory effect in the sample's total resistance.[15] In our work, we observe that certain local regions retain 100% memory, i.e., turn from metallic into insulating phase, or vice-versa, upon performing the ramp-reversal temperature protocol. These observations open up a possibility for future resistivity experiments to contact and probe specific regions in the sample. This could strongly enhance the resistance ramp reversal memory to approach the ultimate resistivity ratio $dR/R \approx 10^4$ of the full metal-insulator transition.

2. Results and Discussion

2.1. Methods

We have developed a new microscopy method to map out clear, stabilized images of the IMT. This optical method allows the precise filming of the transition with hundreds or even thousands of images taken successively. This allows us to track fine details in the time evolution of the metal-insulating patches. The experimental steps necessary to achieve this mapping are detailed in the SI Section S2 and in ref. [19]. In this study, the *ramp reversal protocol* was performed following the one previously used in resistivity measurements by Vardi et al.[15]: 1 major temperature loop spanning the entire IMT (36 °C – 82 °C), followed by 11 hysteresis subloops[20] (59.5 °C – 68 °C) followed by three major temperature loops spanning the entire IMT (see **Figure 1**a).

2.2. Image Average Intensity versus Temperature

Figure 1b reports the spatially averaged 8-bit grayscale optical reflectivity intensity versus temperature of VO_2 obtained during the ramp reversal protocol. The first major loop (black line) shows a clear 1^{st} order hysteretic transition between high and low reflectivity states at temperatures around 65–70 °C, closely resembling the semi-log resistivity curve (see Figure S3, Supporting Information). During the following 11 temperature subloops inside the hysteretic regime (red-graded lines), the reflectivity at temperature TH progressively increases indicating that, on average, fewer metallic domains nucleate in the film after each subloop. When the sample is cooled down deep into the insulating state and a major temperature loop is repeated (green line), the loop's heating branch diverges from the original major loop curve in the vicinity of the turnaround temperature TH (see Figure 1b,d). This constitutes the multi-level ramp-reversal memory effect originally observed in the resistance-temperature experiments.[15] Finally, when the major temperature loop is repeated (cyan and dark blue lines), the original reflectivity curve is restored, i.e., the memory was erased by reaching the fully metallic state. In Figure 1c, we plot reflectivity versus frame number (i.e., Figure 1b as a function of time). The inset displays the intensity at the end of each subloop. The dashed line is the exponential function fit. We find that the increase in overall optical intensity has a characteristic "time constant" of $n_\tau = 3.1 \pm 0.5$ subloop cycles (≈56 min). The previous resistivity study reported an exponential saturation characterized by $n_\tau = 12.8$ subloop cycles (≈4 h). The difference in n_τ could be due to small variations in the sample preparation, a slower temperature ramp rate of the subloops (1K min^{-1} rather than 5–10K min^{-1}) in the optical experiment, or other details such as the exact value of the turning point TH.

2.3. Binary Thresholded Images

For each pixel in the recorded optical images, we track its intensity as a function of time. The midway points of such traces allow us to identify the *frame number*, and therefore the *temperature*, at which each individual pixel switches from insulating to metallic, or from metallic to insulating. Single pixel binary thresholded images were thus generated, identifying insulator and metal patches during the entire temperature protocol (full details of the method are described elsewhere[19]). Figure S3 (Supporting Information) shows a screenshot of the end results as an online movie[21] made up of the full 3500 frames time evolution. This new set of images allows us to: (i) track the spatial location, shape, and time evolution of insulator and metal patches and generate memory maps (Section 2.4); (ii) generate spatial maps (T_c maps) of the local transition temperature (Section 2.5).

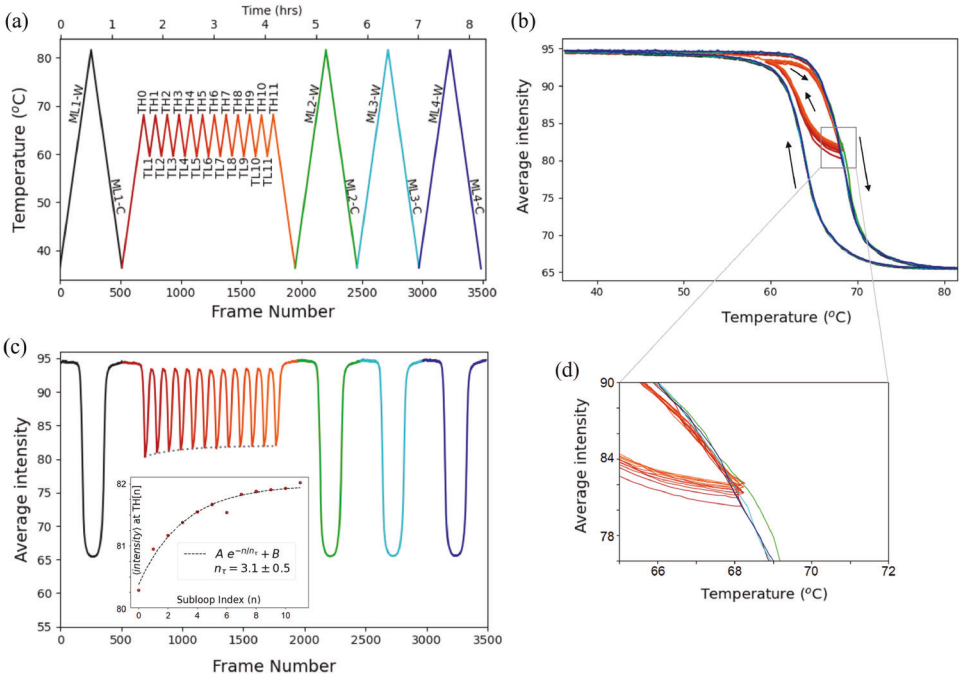

Figure 1. a) Ramp Reversal temperature protocol. Major loop labels are as follows: ML1-W stands for Major Loop One upon warming; ML1-C stands for Major Loop One upon cooling, and similarly for other major loops. In the subloops, temperature is varied repeatedly between a low temperature of TLn = 59.5 °C and a high temperature of THn = 68 °C, through a total of $n = 11$ complete subloops. Black, red/orange, green, cyan, and blue color codes denote the same region of the hysteresis protocol in panels (a–c). b) Hysteresis curves of average intensity versus temperature throughout the Ramp Reversal protocol of panel (a). c) Average intensity versus frame number. Intensity is on a grayscale of 0 (black) to 255 (white), after accounting for illumination variation (detailed elsewhere[19]). The light gray dashed line follows the average intensity at the end of each subloop. Inset: Fit of the average intensity at the end of each subloop (i.e., at THn), versus subloop index n, to an exponential saturation. The time constant is $n_\tau = 3.1 \pm 0.5$ subloops. This rise can be seen in panels (b) and (d) as the bump of the red/orange/green curves. d) Zoom showing the progressive increase after each subloop of the averaged intensity around the high temperature turning point TH = 68 °C.

2.4. Tracking Insulator and Metal Patches at TH

Figure 2 shows the extent to which metallic inclusions flow into the insulator as the temperature is repeatedly ramped up to TH in the 11 memory writing subloops. The top left panel displays the spatial pattern of metal and insulating patches at TH0, before the training subloops begin. Dark gray regions are metallic, and light gray regions are insulating. The next set of panels in Figure 2 (the yellow/blue/gray maps) show the changes in these metal and insulator patches at the end of each of the 11 training subloops. In these "*memory maps*", dark gray indicates regions that are metallic at TH0 *and are also metallic* at the end of the indicated subloop THn. Light grey indicates regions that are insulating at TH0 *and are also insulating* at the end of the indicated subloop. Yellow highlights regions of accumulated memory where metallic inclusions no longer invade the insulator: these are regions that were metallic at TH0 but *remain insulating* at the end of the indicated subloop. Note that a small number of blue regions can also be seen: these are regions that were insulating at TH0, but are now metallic at the end of the indicated subloop. A histogram of each of these colors is reported below the corresponding image. As more subloops are performed, more and more yellow regions (i.e., new insulating patches) accumulate. Blue regions also appear, albeit suddenly compared to the progressive front propagation growth of the yellow regions. These blue regions show at most a weak/decreasing trend with successive subloops as seen in the evolution of the histograms. To summarize, during the 11 memory training subloops, most of the metal (dark gray) and insulating patches (light gray) remain unchanged at the turning point TH. Once an insulating yellow region appears, it tends to grow during successive subloops. By contrast, the few metallic blue regions appearing remain mostly constant in subsequent subloops.

After performing 11 training temperature subloops, we cool the sample deep below T_c, reaching a uniform insulating state (i.e., removing all metallic domains). We repeat the major loop acquisition, ML2, and compare the metal/insulator domain distributions at temperature TH between this loop and at TH0 (panel "Memory probe" ML2(TH)-TH0 in Figure 2). We find a large increase in the insulator domain fraction in the ML2(TH), which indicates that performing the training subloops has altered the path of the phase transition. Comparing TH10-TH0 and ML2(TH)-TH0 maps, we find that yellow patches show a positive correlation of 0.6. This correlation is similar when comparing any THn-TH0 to TH(n-1)-TH0 maps (for $n \geqslant 3$, when exponential ramp reversal memory starts to stabilize). We conclude that the VO_2 sample essentially "memorized" the domain state that was achieved at the end of the last training subloop TH10, even though the domain state was completely reset by cooling down into the insulating state before the ML2 measurement. The subloop memory can, however, be erased by going to high temperature, as can be seen in the rightmost panels of Figure 2, labeled "Reset

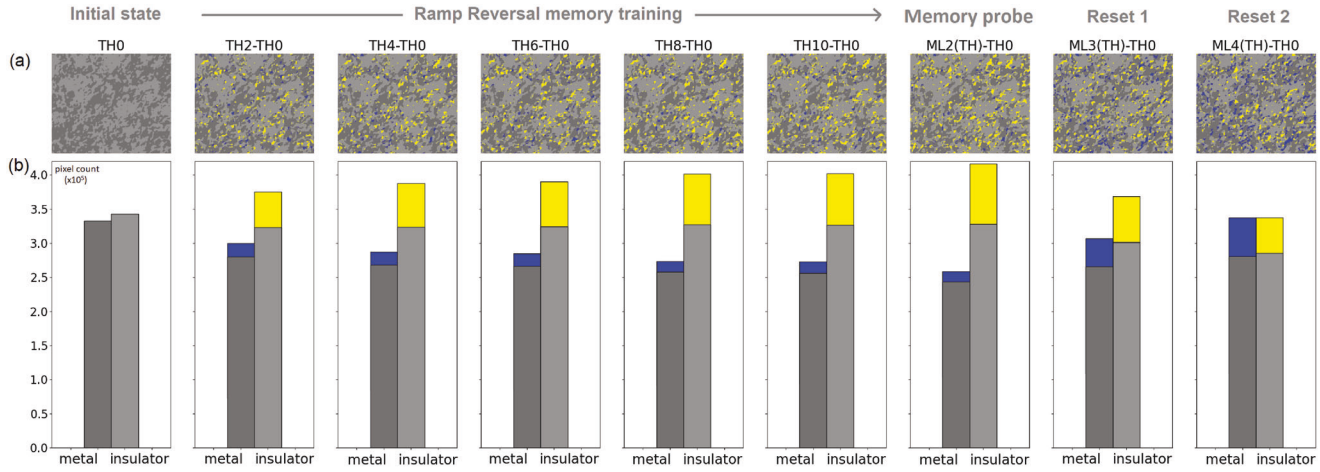

Figure 2. Memory maps: a) Experimental evolution of the spatial map of metal and insulator domains upon training with successive temperature subloops. Top left panel: Metal and insulator patches right before the first subloop begins, at TH0. Metallic patches are colored dark gray, and insulating patches are colored light gray. Image is 28 μm high. Successive panels show the change in metal and insulator domains at the end of every other subloop THn, from $n = 2$ to $n = 10$, with respect to TH0. Pixels that are the same at THn and at TH0 are colored dark grey if they are metallic, and colored light grey if they are insulating. Yellow denotes the growth of insulating patches, and blue denotes the growth of metallic patches. On average, the sample becomes progressively more insulating with subloop training. However, certain regions become metallic with subloop training. ML2(TH)-TH0 (labeled "Memory probe") is the state of the sample with the most accumulated yellow memory patches. In this state, the sample has the highest average T_c as shown in Figure 4d. The top right panels labeled "Reset 1" and "Reset 2" show the difference between ML3-W(TH) and ML4-W(TH) with respect to TH0. Similar figures and statistics are found using ML1(TH) (rather than TH0) as reference as shown in Figure S5 (Supporting Information). Blue pixels in "Reset 1" and "Reset 2" maps are regions that transfer back from insulating to metallic as expected from a memory reset. b) Bottom panels show the corresponding histograms.

1" and "Reset 2". These images compare the metal and insulating patches at TH in ML3-W and ML4-W to TH0. The yellow patches generated in the 11 subloops are erased, i.e., become blue patches in the panels labeled "Reset." The metal/insulating levels return to a ≈ 50/50% state as in TH0. Interestingly, although the global level is reset, the exact locations of the insulating and metal patches are not exactly the same as the initial TH0 map as revealed by the presence of the yellow/blue bars in the ML4 histogram. Generally, when cycling many time through the entire transition in these samples, T_c maps structure do not change globally but only a few domains are modified within $\sigma = 0.6$ °C (see Figure S6, Supporting Information and ref. [19] for more details). The difference between ML4 and ML1 is found to be similar to this natural variation. This indicates that the ramp reversal memory was completely erased after heating the sample to high temperatures within the natural cycle-to-cycle fluctuations found in this material.

To easily see and track the evolution of these new memory patches, we average the yellow/blue maps labeled THn-TH0 in Figure 2a over all subloops. The results of the average are shown in **Figure 3**a. *Red lines* denote the original contours of metal and insulator domains at TH0, before the ramp reversal protocol. The dominant physics evident in this visualization is that during repeated small temperature reversals, the insulator advances further into metallic clusters, and that it does so primarily via front propagation. Figure 3a also makes it clear that in the VO_2 thin film, the ramp reversal protocol not only induces new insulating regions, but it also creates several new metallic blue regions that were not previously present. That is, while the *average* transport characteristics become more insulating, there are certain regions where the sample becomes more metallic and remains so during the ramp reversal protocol. This effect was not foreseen in the scar model, since the phenomenon is not evident via macroscopic transport measurements, and can only be detected by a spatially resolved probe that is sensitive to the local conductivity.[15] There are also several blue regions from Figure 2a that become very faint during the averaging process of Figure 3a. These could either be transients due directly to the dynamics, or they could be fleeting thermal fluctuations.

2.5. Local Transition Temperature Maps - T_c Maps

The determination of the intensity midway points for each single pixel also allows us to construct spatial maps of the local transition temperature (T_c maps) for each temperature ramp. **Figure 4**a shows the spatial maps of the local transition temperature T_c of the sample during major loop warming runs before the training subloops (ML1-W), and just after performing the 11 ramp reversal training subloops (ML2-W) (see Figure S8, Supporting Information for a higher resolution version, and also for ML3-W and ML4-W T_c maps after cycling to high temperatures to reset the system). The ML2-W local T_c map reveals the accumulated *ramp reversal memory* as increased ruggedness in the T_c map (i.e., the distribution of T_c has become broader) and a shift of the average T_c to a slightly higher value. These two metrics return to their initial ML1-W levels after heating the sample to high ($T \gg T_c$) temperatures as shown in Figure 4d. To complement the histograms in Figure 4c, Figure S7 (Supporting Information) shows a *spatial* visualization to track the difference between ML1-W and ML2-W. This figure presents a *four*-color map identifying whether regions that originally have higher-than-average T_c increase or

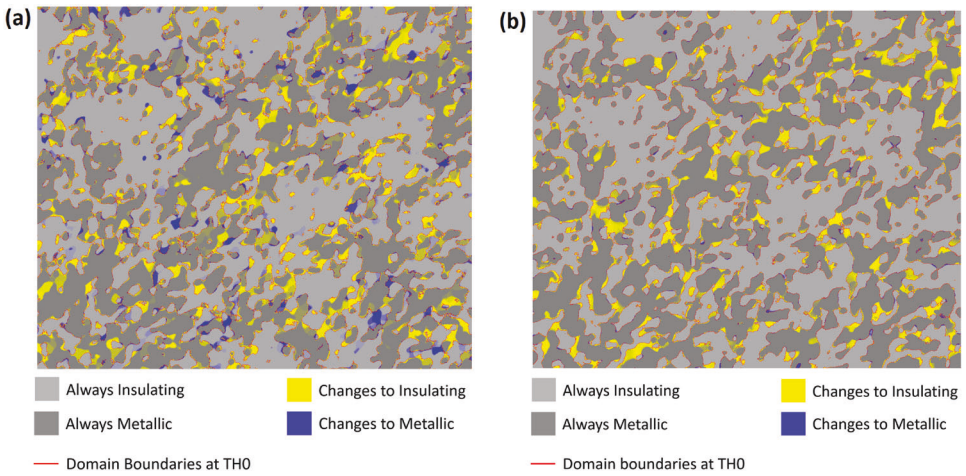

Figure 3. Accumulated memory maps: a) Experimental and b) simulated averaged metal and insulator domains at the end of each subloop. The images are a direct average over ten subloops of the THn-TH0 images. Dark gray denotes regions that are metallic at TH; light gray denotes regions that are insulating at TH. Yellow regions are places where the insulator advanced as compared to TH0. Blue regions are places where the metal advanced as compared to TH0. Light yellow regions are typically regions that became insulating only at the end of the ten subloops. Bright yellow regions however are regions that became insulating at the beginning of the subloops. Red contours mark the original metal-insulator boundaries at TH0, before the subloops begin.

decrease their T_c during ramp reversal, and likewise for lower-than-average T_c regions. The fact that all four possibilities are present in an inter-twinned manner reveals the complexity of the memorization process.

Overall, by analyzing the experimental T_c maps, we arrive at an important conclusion: upon performing training subloop temperature cycles, the memory accumulates throughout the entire VO_2 film, and not just at the domain boundaries as was proposed in the original scar model.[15]

2.6. Minimal Model of Point Defect Motion

While the scar model offers a plausible explanation of the macroscopic resistivity curves, the spatially resolved optical microscopy maps acquired here necessitate a new model, capable of explaining the accumulation of memory deep inside metallic and insulating patches, and capable of explaining why certain regions in the sample have a *lowered* T_c rather than a raised T_c (for a detailed comparison between the scar model and optical memory maps, see Section S5, Supporting Information).

We propose that diffusion of point defects in the metal-insulator phase separation regime can account for the ramp reversal effects observed in both macroscopic resistivity measurements and the optical microscopy measurements presented here. We assume that there is a class of point defects that diffuse during the ramp reversal process. Because the ramp reversal process induces phase segregation between metal and insulator, this necessitates a treatment that goes beyond the standard diffusion equation. We use the diffusion-segregation equation (see Equation 9 of ref. [22]) to describe defect motion in the presence of phase segregation into metal and insulator domains:

$$\frac{\partial \rho}{\partial t} = \frac{\partial}{\partial x}\left[D(x)\left(\frac{\partial \rho}{\partial x} - \frac{\rho}{\rho_{\mathrm{eq}}}\frac{\partial \rho_{\mathrm{eq}}}{\partial x}\right)\right] \quad (1)$$

For a given position and conformation of the metal-insulator boundary, we know that as $t \to \infty$, we will recover the equilibrium solution to this differential equation, $\rho(t \to \infty) \to \rho_{\mathrm{eq}}(x)$. Note that the overall scale of the equilibrium density ρ_{eq} is not important, because the equation is invariant under the transformation $\rho_{\mathrm{eq}}(x) \to C\rho_{\mathrm{eq}}(x)$ where C is a uniform scalar. However, the spatial dependence of ρ_{eq} is important, since $\rho_{\mathrm{eq}}^{\mathrm{metal}} \neq \rho_{\mathrm{eq}}^{\mathrm{insulator}}$. Therefore, we only need (as input) the ratio $\rho_{\mathrm{eq}}^{\mathrm{insulator}}/\rho_{\mathrm{eq}}^{\mathrm{metal}} \equiv s$ where s is known as the "segregation coefficient".[23,24] The relative concentration of defects at long times is ultimately set by the difference in the Gibbs free energy formation of the defects[22,25] in the metal and insulator phases (see SI). In what follows, we assume that $s < 1$. This assumption (discussed in Section S7, Supporting Information) leads to defects gathering in the metal throughout the ramp reversal process, while defects are depleted from the insulator, anytime there is phase segregation of metal and insulator domains. In addition, as metal clusters shrink while the temperature is being lowered, they transport defects with them.[23,24,26] This process of cleaning defects from the rest of the sample is similar to the floating zone melting technique used to purify semiconductors. This means that over repeated iterations of the ramp reversal protocol, defects are moved out of the original locations of the insulator patches at TH0, toward the regions of lowest T_c in the sample. Because defects generically lower transition temperatures, this transport of defect out of the insulating regions and into the metallic regions has the net effect of increasing the transition temperature in the cleaner regions of the sample (the insulator), and of lowering it in the regions with higher defect concentration (the metal). Overall, this makes the transition temperature maps more rugged, as seen in the ML2-W panel of **Figure 5**d. Rather than changing abruptly, the equilibrium concentration of these mobile defects must change smoothly at a metal-insulator boundary. Therefore, we have set ρ_{eq} to be a step function convolved with a gaussian kernel of width ξ, and we use

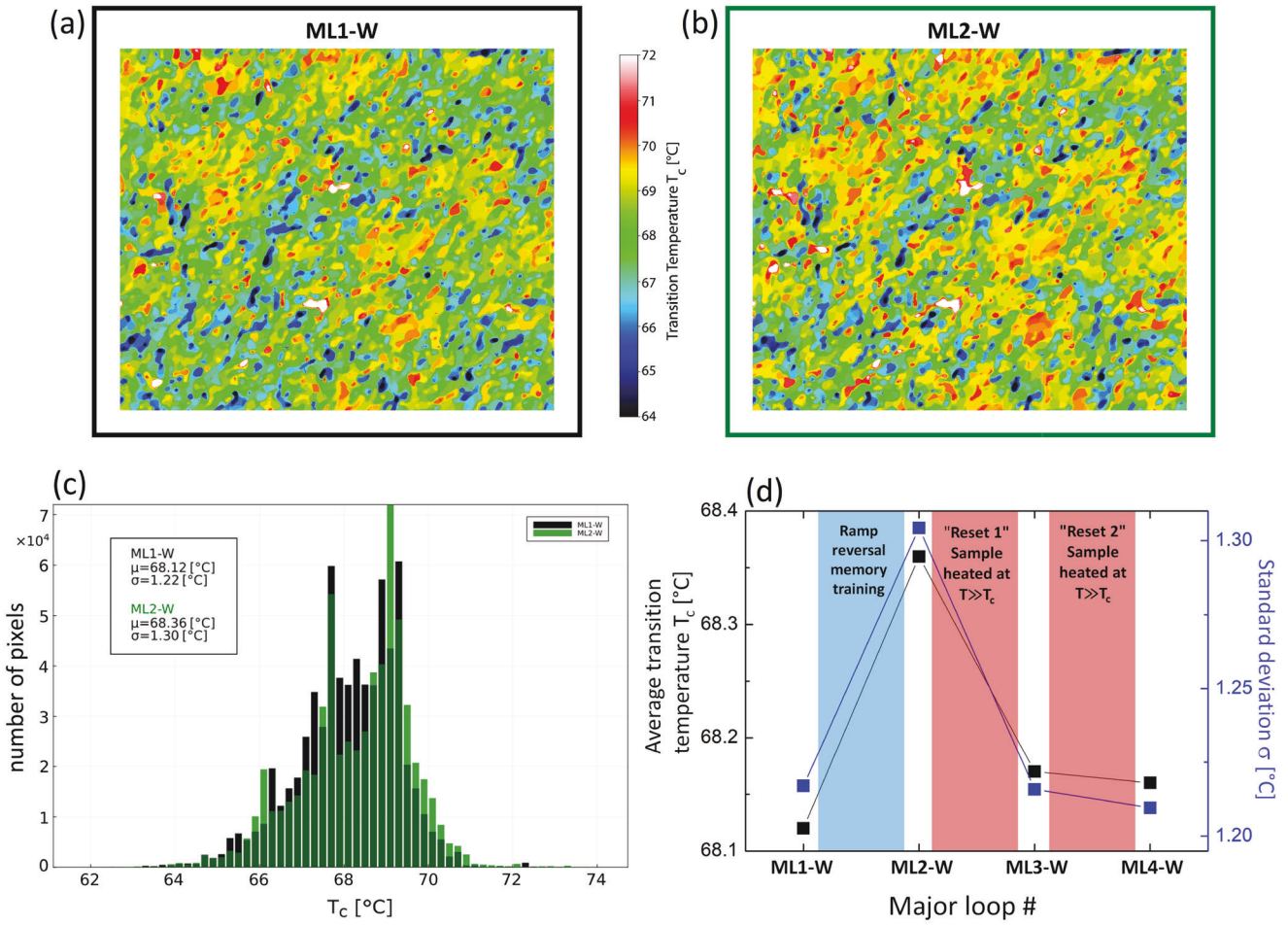

Figure 4. Panel a): T_c map acquired during the warming branch of the first major loop (called ML1-W). Panel b): T_c map acquired during the warming branch of the second major loop (ML2-W) after 11 small subloops memory training. c) Histograms of ML1-W and and ML2-W maps. Histograms of ML3-W and and ML4-W are presented in Figure S9 (Supporting Information). d) Plot of the average transition temperature and standard deviation for all four major loops. Error bars are ±0.002 °C. They are smaller that the symbol size and much smaller than the changes observed. The increase of both T_c and the standard deviation σ (ruggedness) of ML2-W reveals that these two quantities are good metrics of the ramp reversal memory state.

the minimum width ($\xi = 5$) needed to suppress artifacts associated with an overly abrupt change in ρ_{eq}.

To initialize the calculation, we use the T_c map from Figure 1d obtained experimentally from the warming branch of the first major loop (ML1-W) as the input to our model, and follow the temperature protocol shown in Figure S10 (Supporting Information). The density of defects at the beginning of ML1-W is adjusted using the gradient descent method, so that when the model undergoes the first warming procedure ML1-W, the T_c map we get is identical to ML1-W in Figure 1d. This ensures that, starting from the end of ML1-W, our model will go through the same process as the experiment reported in Figure 1, starting from the same initial conditions.

2.7. Comparison of Theoretical Results to Experimental Results

Figures 5a shows how the metal and insulator domains change during the ramp reversal protocol. Like the experimental results of Figure 2, we observe that yellow patches (regions that were originally metallic at TH0 but change to insulating during the temperature subloops) advance further and further with each iteration, via domain wall propagation.

Figures 5c and Figure S10b (Supporting Information) show how the fraction of the total area occupied by insulator (A_i) changes over time in the simulation. The metallic fraction $A_m = 1 - A_i$ can be linearly mapped to the inset of Figure 1c under the simplifying assumption $I_{total} = A_m I_m + (1 - A_m) I_i$. As with the experimental result, the simulation also predicts saturation of the theoretical insulating fraction during the ramp reversal protocol. A fit of the theoretical change in insulating fraction to an exponential saturation with subloop index is shown in Figure 5c, yielding $n_\tau = 3.0 \pm 0.2$ subloops, in agreement with the experimental result shown in the inset of Figure 1c. The time constant n_τ depends on the parameters chosen in the model, including the value of the segregation coefficient and diffusion constants (see Table S1, Supporting Information).

In Figure 3b, we show the theoretical accumulated phase change maps according to the defect motion model. These are an average over ten subloops of the yellow/blue maps of the

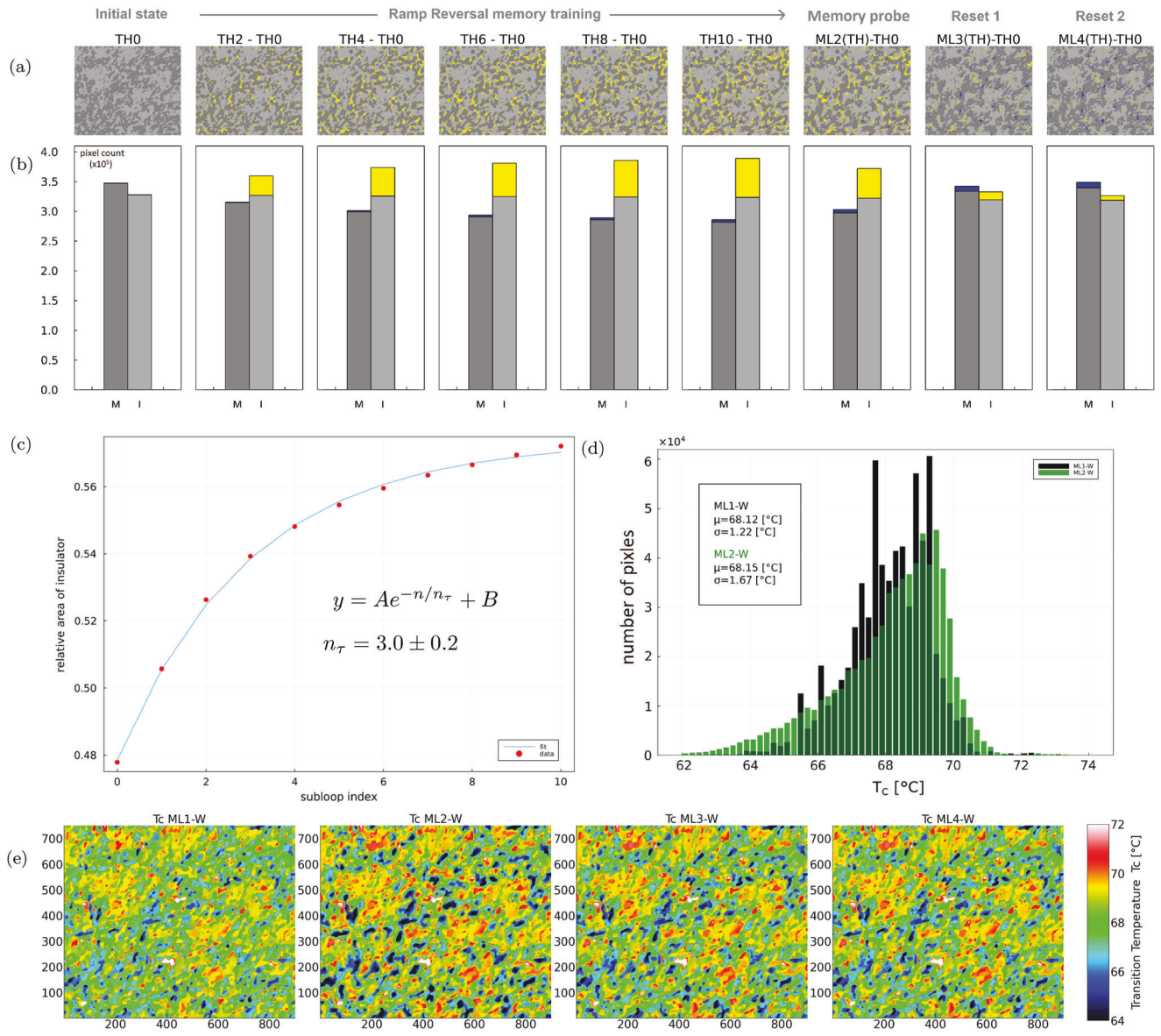

Figure 5. Theoretical prediction of the evolution of metal and insulator domains during the ramp reversal protocol, computed according to Equation 1. Parameters used to generate this result are listed in Figure S10 (Supporting Information). a) Successive panels show the change in metal and insulator domains at the end of the even numbered subloops THn, from n = 2 to n = 10, with respect to TH0. Pixels that are the same at THn and at TH0 are colored dark grey if they are metallic (M), and colored light grey if they are insulating (I). Yellow denotes the growth of insulating patches relative to TH0, and blue denotes the growth of metallic patches. Figure 3 shows an averaged version from TH1-TH0 to TH10-TH0. b) Histograms of the area of each colored region from (a). The area covered by insulating (yellow) patches increases progressively during the ramp reversal protocol, in agreement with the experimental results of Figure 2. c) Fit of the total number of insulating sites at the end of each subloop (i.e., at THn), vs. subloop index n, to an exponential saturation. Red dots: original data from model; Blue line: fitted exponential curve $y = Ae^{-n/n_\tau} + B$. The time constant is $n_\tau = 3.0 \pm 0.2$ subloops. d) Histograms of T_c maps ML1-W and ML2-W to be directly compared to the experimental histograms presented in Figure 4(c). e) Theoretical T_c maps for the four major loops upon warming.

subloops THn-TH0 shown in Figure 5a. In common with the experimental results, the dominant physics is that the insulator advances farther and farther into the metallic clusters during repeated temperature reversals, primarily via front propagation. Whereas in the thin film of VO_2, Figure 3a shows that there are places where the metal clusters also advance and remain during the ramp reversal protocol, by contrast, the blue regions in the simulation (Figure 2a) and 3b) are almost all *transients*. In the simulation, these arise primarily near the metal-insulator boundaries, in regions where the boundary is most jagged. Transients are a ubiquitous effect in driven systems before they have reached a stable limit cycle.[27] Note that none of the transient effects in the simulation are attributable to thermal fluctuations, since the simulation involves only the deterministic time evolution of a differential equation with a driving term (the change in temperature), but there are no stochastic terms.

While the theory and experiment agree in broad strokes, the specific locations of the new insulating regions predicted in panel (b) of Figure 3 do not match exactly the experimental results summarized in panel (a). One reason is that we do not know the underlying distribution of mobile defects, but we have only inferred it from the experimental T_c map derived from ML1-W. This is at best an indirect measurement of the mobile defects, since the experimental T_c map is also sensitive to, e.g., defects and strain fields from the substrate that are not mobile at these temperatures. Moreover, because the theoretical defect density was initialized by optimizing the resulting T_c map for ML1-W and not for the location of the red boundaries, the red boundaries, while mostly similar, show some differences. In addition, the maps in Figure 3 are sensitive to the exact timing with which an individual region changes from metal to insulator (or vice versa) during the ramp reversal protocol. For example, the few places where the red lines are different between theory and experiment are regions where the experimental system changed to insulator before the theoretical one, or vice versa. Since the yellow/blue colorations are drawn relative to the red demarcations, the yellow/blue maps are sensitive to these small differences in their exact location.

Both theory and experiment show that regions of high T_c get higher as a result of the ramp reversal protocol. However, while the theory predicts that regions of low T_c should become lower during the ramp reversal protocol (because these regions gather the most defects), this is not seen in the experiment. Rather, in experiment the low T_c's do not all become lower, and the average T_c increases in going from ML1-W to ML2-W. This difference could have several origins, including the following: i) We assumed a linear mapping between changes in T_c and changes in the local defect density. A nonlinear mapping could account for the difference. ii) Annealing can also decrease the effective disorder. A combination of increased defects in the metallic regions along with annealing the positions of those defects as the metallic clusters "breathe" during the 11 subloops (see video [21]) could lead to a null effect on the local T_c. iii) Regions with defect concentration already near ρ_{eq} cannot adjust much during the ramp reversal protocol. Indeed, it could be that the original metallic regions in ML1-W are already close to the saturation defect density. iv) Finally, certain types of defects, such as oxygen interstitials and vacancies, can exchange with the surrounding air, an effect that was not included in our model. Indeed, while our model is based largely on thermodynamic considerations and requires minimal assumptions, further microscopic theoretical work would be needed to predict which species of point defect, if any, may be contributing.

It is possible that a different combination of input parameters to the defect mobility model may favor the growth of metallic domains in addition to the insulating domains, as happens in Figure 3a. However, there are certain features evident in this current dataset as well as the broader literature that point toward the importance of interactions, which are not included in our defect mobility model. First, our prior analysis of a similar VO_2 thin film measured by s-SNIM showed that interactions are a key driver in the geometry of patterns made by metal and insulator patches during the IMT.[28] Second, the presence of resistance jumps[29] in mesoscopic geometries is strongly suggestive that when one region undergoes a phase change from metal to insulator or vice versa, this can trigger neighboring regions to do likewise as expected from previous work showing avalanches in this material.[29] Indeed, true avalanches (as opposed to simultaneous but independent switching events) are impossible without interactions. Finally, the compact nature of the blue regions in Figure 3a is highly suggestive of interactions. Clusters that form in the absence of interactions (as happens, for example, in percolation theory) are more rarefied, whereas interacting clusters are more compact.[30,31] In summary, while the defect motion model captures much of the ramp reversal memory effect, future work should explore the interplay of this physics with interactions.

Note that the optical experiments in this paper provide at most indirect evidence of defect movements in the sample. However, within the limitations cited above, the proposal of point defect diffusion provides new insights into possible experiments that could be conducted in the future, such as ramp reversal seen by local probes (STM, SNOM, etc.), the effect of film/substrate strain, film thickness, and temperature ramp time on ramp reversal memory. These experiments will help to further constrain the models proposed so far (scar model, defect motion model), but are outside the scope of this paper.

3. Conclusion

In conclusion, we have reported the first optical imaging of ramp reversal memory in VO_2. Multiple new experimental steps were needed to align, focus and calibrate the raw grayscale images recorded. These experimental achievements allowed us to accurately track the spatial distribution of metal and insulator clusters and to study their evolution during the thermal subloop training sequence. In successive and accumulated memory maps, we find that clusters evolve by front propagation from one subloop to the next. After all subloops, the transition temperature map is more rugged, revealing that memory accumulates not only at the cluster boundaries at TH, but memory also accumulates deep inside the metal and insulator patches over the entire sample. Based on thermodynamic considerations, we propose that preferential diffusion of point defects into metal domains throughout the ramp reversal process could account for the observed memory accumulation throughout the entirety of the film. Because these metal domains transport defects with them each time they shrink, local transition temperatures decrease where the metal droplets spend the most time, and increase in the regions that are always insulating. This ultimately leads to the metal inclusions advancing over less territory with successive ramp reversals. Further work would be needed to identify that species of defects are contributing. We find that the subloop-trained memory disappears as expected after raising the sample to a high temperature T = 82 °C, just above the closing of the major hysteresis loop. Mapping other materials that have also shown ramp reversal memory[15,18] and other IMT materials in general would be useful to test universality of our observations and the defect motion model, which was developed. The observation of spatially resolved nonvolatile memory encoding in VO_2 paves the way toward developing multi-level memory synaptors for neuromorphic computing applications. In addition, the proposed connection between ramp reversal memory and defect mobility opens up the possibility to enhance the memory effect via defect engineering methods by, e.g., using dopants or ion irradiation, or by tuning the material synthesis conditions.

Supporting Information

Supporting Information is available from the Wiley Online Library or from the author.

Acknowledgements

The authors thank M. J. Carlson for technical assistance with image stabilization, and acknowledge helpful conversations with K. A. Dahmen. S.B., F.S., and E.W.C. acknowledge support from NSF Grant no. DMR-2006192 and the Research Corporation for Science Advancement Cottrell SEED Award. S.B. acknowledges support from a Bilsland Dissertation Fellowship. E.W.C. acknowledges support from a Fulbright Fellowship and from DOE BES Award no. DE-SC0022277, and thanks the Laboratoire de Physique et d'Étude des Matériaux (LPEM) at École Supérieure de Physique et de Chimie Industrielles de la Ville de Paris (ESPCI) for hospitality. This research was supported in part through computational resources provided by Research Computing at Purdue, West Lafayette, Indiana.[32] The work at UCSD (PS, IKS) was supported by the Air Force Office of Scientific Research under award number FA9550-20-1-0242. The work at ESPCI (M.A.B., L.A., and A.Z.) was supported by Cofund AI4theSciences hosted by PSL University, through the European Union's Horizon 2020 Research and Innovation Programme under the Marie Skłodowska-Curie Grant no. 945304.

Conflict of Interest

The authors declare no conflict of interest.

Data Availability Statement

The data that support the findings of this study are available from the corresponding author upon reasonable request.

Keywords

defect motion, memory, memristors, metal-insulator transition, mott transition, phase separation

Received: February 7, 2023
Revised: April 15, 2023
Published online: July 10, 2023

[1] M. Imada, A. Fujimori, Y. Tokura, *Rev. Mod. Phys.* **1998**, *70*, 1039.
[2] Z. Yang, C. Ko, S. Ramanathan, *Annu. Rev. Mater. Res.* **2011**, *41*, 337.
[3] F. J. Morin, *Phys. Rev. Lett.* **1959**, *3*, 34.
[4] M. Fäth, S. Freisem, A. A. Menovsky, Y. Tomioka, J. Aarts, J. A. Mydosh, *Science* **1999**, *285*, 1540.
[5] K. McElroy, J. Lee, J. A. Slezak, D.-H. Lee, H. Eisaki, S. Uchida, J. C. Davis, *Science* **2005**, *309*, 1048.
[6] M. M. Qazilbash, M. Brehm, B.-G. Chae, P.-C. Ho, G. O. Andreev, B.-J. Kim, S. J. Yun, A. V. Balatsky, M. B. Maple, F. Keilmann, H.-T. Kim, D. N. Basov, *Science* **2007**, *318*, 1750.
[7] K. W. Post, A. S. McLeod, M. Hepting, M. Bluschke, Y. Wang, G. Cristiani, G. Logvenov, A. Charnukha, G. X. Ni, P. Radhakrishnan, M. Minola, A. Pasupathy, A. V. Boris, E. Benckiser, K. A. Dahmen, E. W. Carlson, B. Keimer, D. N. Basov, *Nat. Phys.* **2018**, *14*, 1056.
[8] H. Kuwamoto, J. M. Honig, J. Appel, *Phys. Rev. B* **1980**, *22*, 2626.
[9] M. Coll, J. Fontcuberta, M. Althammer, M. Bibes, H. Boschker, A. Calleja, G. Cheng, M. Cuoco, R. Dittmann, B. Dkhil, I. E. Baggari, M. Fanciulli, I. Fina, E. Fortunato, C. Frontera, S. Fujita, V. Garcia, S. Goennenwein, C.-G. Granqvist, J. Grollier, R. Gross, A. Hagfeldt, G. Herranz, K. Hono, E. Houwman, M. Huijben, A. Kalaboukhov, D. Keeble, G. Koster, L. Kourkoutis, et al., *Appl. Surf. Sci.* **2019**, *482*, 1.
[10] J. del Valle, P. Salev, Y. Kalcheim, I. K. Schuller, *Sci. Rep.* **2020**, *10*, 4292.
[11] W. Yi, K. K. Tsang, S. K. Lam, X. Bai, J. A. Crowell, E. A. Flores, *Nat. Commun.* **2018**, *9*, 4661.
[12] M. Ignatov, M. Ziegler, M. Hansen, A. Petraru, H. Kohlstedt, *Front. Neurosci.* **2015**, *9*, 316.
[13] S. Oh, Y. Shi, J. del Valle, P. Salev, Y. Lu, Z. Huang, Y. Kalcheim, I. K. Schuller, D. Kuzum, *Nat. Nanotechnol.* **2021**, *16*, 680.
[14] S. Cheng, M.-H. Lee, X. Li, L. Fratino, F. Tesler, M.-G. Han, J. del Valle, R. C. Dynes, M. J. Rozenberg, I. K. Schuller, Y. Zhu, *PNAS* **2021**, *118*, e2013676118.
[15] N. Vardi, E. Anouchi, T. Yamin, S. Middey, M. Kareev, J. Chakhalian, Y. Dubi, A. Sharoni, *Adv. Mater.* **2017**, *29*, 1605029.
[16] M. S. Nikoo, R. Soleimanzadeh, A. Krammer, G. M. Marega, Y. Park, J. Son, A. Schueler, A. Kis, P. J. W. Moll, E. Matioli, *Nat. Electron.* **2022**, *5*, 596.
[17] J. del Valle, J. G. Ramírez, M. J. Rozenberg, I. K. Schuller, *J. Appl. Phys.* **2018**, *124*, 211101.
[18] E. Anouchi, N. Vardi, Y. Kalcheim, I. K. Schuller, A. Sharoni, *Phys. Rev. B* **2022**, *106*, 20.
[19] M. A. Banguero, S. Basak, N. Raymond, F. Simmons, P. Salev, I. K. Schuller, L. Aigouy, E. W. Carlson, A. Zimmers, *arXiv:2301.04220*, **2023**.
[20] Subloops are referred to as minor loops or nested loops depending on the field of research.
[21] Online movie: "Thin Film Vanadium Dioxide undergoing Insulator-Metal Transition", https://youtu.be/k21Tb1U1r78.
[22] H.-M. You, U. M. Gösele, T. Y. Tan, *Jpn. J. Appl. Phys.* **1993**, *74*, 2461.
[23] M. M. Atalla, E. Tannenbaum, *Bell Syst. Tech. J.* **1960**, *39*, 933.
[24] F. Bailly, M. Barbé, G. Cohen-Solal, D. Lincot, *J. Phys.* **1983**, *44*, 489.
[25] L. D. Landau, E. M. Lifshitz, *Course of Theoretical Physics*, Butterworth-Heinemann **1980**.
[26] J. G. Ramirez, T. Saerbeck, S. Wang, J. Trastoy, M. Malnou, J. Lesueur, J.-P. Crocombette, J. E. Villegas, I. K. Schuller, *Phys. Rev. B* **2015**, *91*, 205123.
[27] H. Poincaré, *Comptes rendus hebdomadaires de l'Académie des sciences de Paris* **1880**, *90*, 673.
[28] S. Liu, B. Phillabaum, E. Carlson, K. Dahmen, N. Vidhyadhiraja, M. Qazilbash, D. Basov, *Phys. Rev. Lett.* **2016**, *116*, 036401.
[29] A. Sharoni, J. G. Ramírez, I. K. Schuller, *Phys. Rev. Lett.* **2008**, *101*, 026404.
[30] L. Burzawa, S. Liu, E. W. Carlson, *Phys. Rev. Mater.* **2019**, *3*, 033805.
[31] B. Phillabaum, Ph.D. thesis, Purdue University, West Lafayette **2012**.
[32] T. Hacker, B. Yang, G. McCartney, *Educ. Rev.* **2014**.